

Resonant waveguide grating imager for live cell sensing

Ann M. Ferrie, Qi Wu,^{a)} and Ye Fang^{b)}

Biochemical Technologies, Science and Technology Division, Corning Incorporated, Corning, New York 14831, USA

(Received 24 October 2010; accepted 8 November 2010; published online 1 December 2010)

We report on a resonant waveguide grating imager for high throughput screening using live cells. This imager can generate a snapshot image of all biosensors in a 384-well microtiter plate with a time resolution of ~ 3 s and a spatial resolution of $80 \mu\text{m}$. This imager is well tolerant to variability in plate configurations and cell confluency. The resonant wavelength and its shifts induced by cell responses at each pixel correlate well with cell confluency. Data filtration protocol can be used to improve assay quality for partially confluent cells. © 2010 American Institute of Physics. [doi:10.1063/1.3522894]

Resonant waveguide grating (RWG) biosensor is a nanograting waveguide-based optical biosensor that has attracted much interest for cell-based assays in recent years¹⁻³ because it enables noninvasive, sensitive, and integrative measures of cell signaling based on stimulus-induced dynamic mass redistribution (DMR) in live cells.⁴⁻¹¹ Conventional systems employ a stationary array of fiber optics to repetitively scan a microtiter plate.¹² As a result, only cells along the scanning path ($\sim 100 \mu\text{m}$ in width) are sampled to generate an averaged response.¹³ This, in turn, not only smooths out certain rapid responses such as cell micromotion and heart cell beating but also could introduce assay variability due to biosensor defects and nonuniform cell confluency.¹³ Thus, current biosensor cellular assays recom-

mend the use of confluent cell monolayer,³ which could be difficult to achieve for certain cell types (e.g., primary cells and stem cells). To address these issues, we report on a whole microtiter plate RWG imager for high throughput screening (HTS) using live cells.

Figure 1(a) illustrates the schematic of a RWG imager for whole cell sensing. A tunable light source is passed through a polarizer to generate polarized light, which then sequentially passes through a lens L1 and a beam splitter. The split light with a narrow bandwidth is then expanded via another lens L2 and hits on a folding mirror, leading to a reflected light that simultaneously illuminates at a normal incident angle all biosensors within a 384-well Epic[®] microtiter plate (Corning Inc., Corning, NY). The tunable light

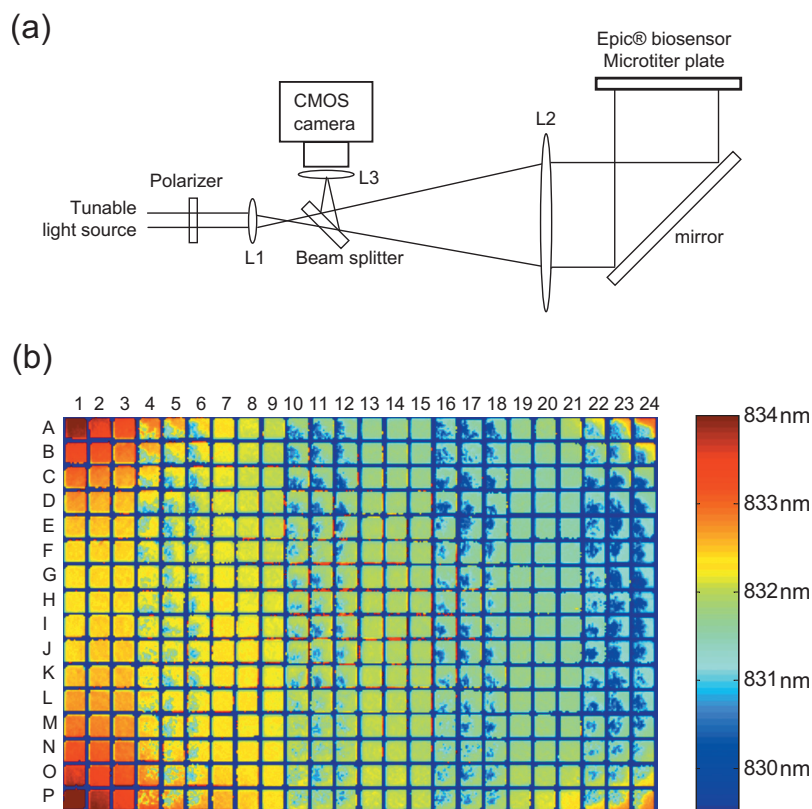


FIG. 1. (Color) A RWG imager. (a) The imager consists of three components: a tunable light source to sweep the wavelength range, an array of optical components to guide and expand light path leading to illuminate at a normal incident angle all biosensors within a plate, and a CMOS camera to record the resonant wavelength image. (b) A false-colored λ_r image of a whole 384 well Epic[®] biosensor plate having cultured A431 cells.

^{a)}Electronic mail: wuq@corning.com.

^{b)}Electronic mail: fangy2@corning.com. Tel.: +607-9747203. FAX: +607-9745957.

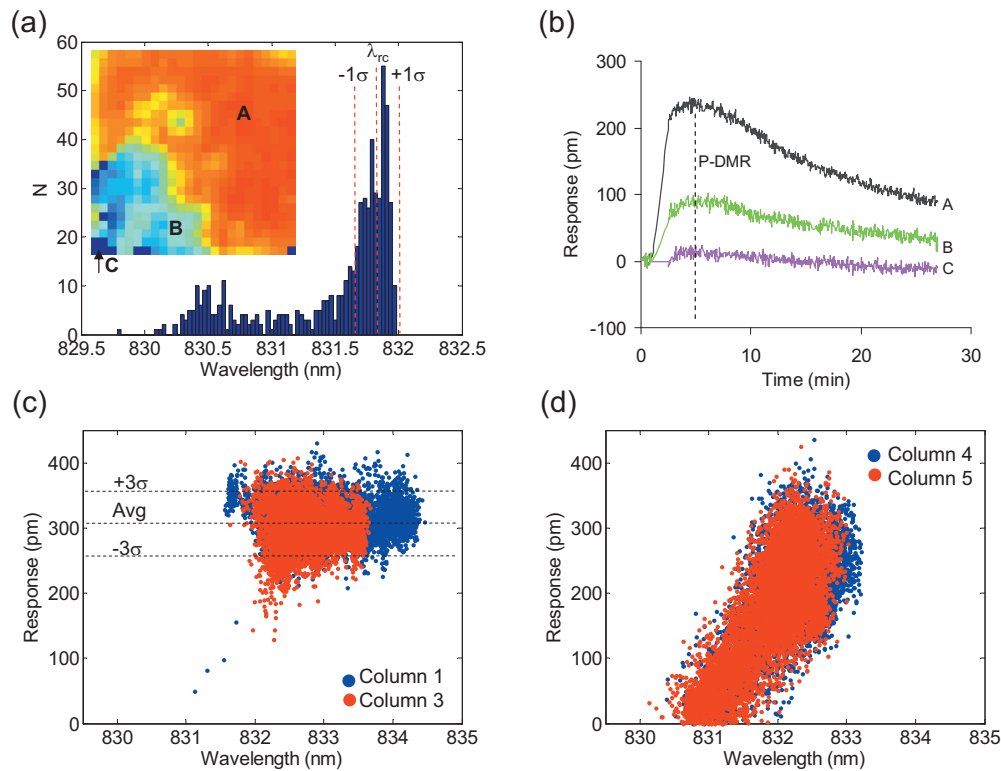


FIG. 2. (Color) Characterization of the RWG imager. (a) The basal λ_r image (inset) and distribution of a biosensor having partial cell coverage. The λ_r values were binned for every 25 pm. (b) The kinetic responses to histamine at 3 pixels [A, B, and C in (a)]. The DMR amplitude is also indicated as P-DMR (positive-DMR). [(c) and (d)] The correlation between the histamine DMR amplitude and its corresponding basal λ_r value for fully and partially confluent cells, respectively.

source rapidly sweeps the wavelength range such that light at a specific wavelength is coupled into the waveguide and is eventually reflected back via a leaky mode. The central wavelength (i.e., resonant wavelength λ_r) of the reflected light is tracked and recorded using a 1400×1024 pixel complementary metal-oxide semiconductor (CMOS) camera (Dalsa Inc., Ontario, Canada). Thus, the λ_r values at all locations are simultaneously collected to generate a pixelated image with a spatial resolution of $80 \mu\text{m}$. The λ_r values before cell stimulation is termed the basal resonant wavelength. The cellular response upon stimulation is monitored in real time as the wavelength shift (in picometer, pm) after all basal λ_r values are normalized to zero. This imager exhibits low thermal noise (0.18 ± 0.03 pm, $n=384$) for the whole plate under ambient conditions, comparable or better than conventional systems.

Figure 1(b) shows a basal λ_r image of a biosensor plate obtained after overnight culturing of human epidermal carcinoma A431 cells. The initial cell seeding numbers were alternated every three columns. For columns 1–3, 7–9, 13–15, and 19–21, 20 000 cells per well were plated such that after culture the cells form a confluent monolayer. For other columns, 6000 cells per well were seeded to form partially confluent layer. It is obvious from the image that there is significant difference in λ_r value, which is due to plate configurations and/or cell confluency. First, the λ_r value, in overall, gradually decreases from left to right across the plate mostly due to the uneven positioning of the plate relative to the incident light plane. Second, the corner wells seem have higher λ_r than the central wells mostly due to the difference in cells resulted from different culture environments (commonly known as the edge well effect). Finally, the λ_r distri-

bution is uniform for the sensors having confluent cells but uneven for others having partially confluent cells. Figure 2(a) shows an λ_r image of a biosensor with partial cell coverage [the well 11D in Fig. 1(b)]. The λ_r distribution is correlated well with light microscopic image (data not shown) and contains largely one peak centered on a high λ_r value (λ_{rc}) corresponding to pixels having large or continuous patches of cell monolayer, suggesting that the anchorage of cells indeed increases the λ_r .

To examine the imager performance, the dependence of apparent cellular responses on cell confluency was examined. The cells in columns 1–6 were stimulated with histamine at a fixed dose ($5 \mu\text{M}$). Histamine is the natural agonist of endogenous G_q -coupled histamine receptor subtype 1 in A431.¹⁴ Figure 2(b) shows the kinetic responses to histamine at three locations, as indicated as A, B, and C in the inset image of Fig. 2(a), all within the same biosensor. The A, B, and C pixels have a high, medium, and low λ_r value, respectively. The cellular response at A is the highest, while at C, there is no any histamine response, suggesting that the apparent histamine response depends on cell confluency. This is expected since the imager has a resolution of $80 \mu\text{m}$ and thus cannot resolve single cells ($\sim 15 \mu\text{m}$). The higher numbers of cells for a given pixel, the greater λ_r value and cellular response.¹⁵

Variability in cell confluency is common to typical HTS campaigns. Thus, we were interested in data filtration methods for improving HTS data quality using the imager. Figures 2(c) and 2(d) show the correlation analysis between the histamine response and the basal λ_r value at each pixel. Results show that for confluent cells the histamine response is

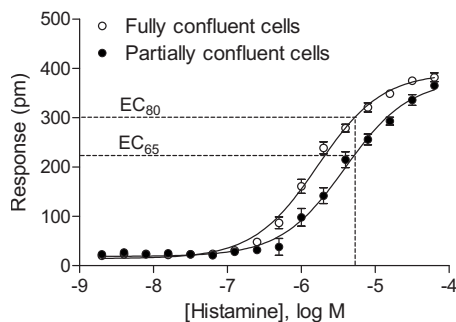


FIG. 3. The relation between the histamine doses and their DMR amplitudes. For fully confluent cells the data are nonfiltered, while for partially confluent cells, the data were calculated after filtration using the $\lambda_{rc} \pm 1\sigma$ matrix.

mostly insensitive to the λ_r value—the averaged amplitudes of all pixels within both columns 1 and 3 are identical (309 ± 16 pm) and $\sim 95\%$ of all responses fall into the 3σ range [Fig. 2(c)]. This suggests that the imager is well tolerant to the abovementioned variability in biosensor plate configurations, and the use of confluent cells can indeed lead to robust assays. Conversely, for partially confluent cells, the histamine DMR amplitude increases linearly as the λ_r value increases [Fig. 2(d)], suggesting that regardless of cell numbers per pixel, the histamine response at single cell level is largely the same. Fitting the λ_r distribution shown in Fig. 2(a) with Gaussian led to an λ_{rc} value with a standard deviation σ . Calculating the cellular responses at pixels having an λ_r value within the $\lambda_{rc} \pm 1\sigma$ range led to an averaged response of 239 ± 16 pm, greater than that of all pixels (201 ± 26 pm). Using the $\lambda_{rc} \pm 1\sigma$ as a filtration matrix, the histamine response for all wells in columns 4–6 was 235 ± 12 pm ($n=48$), which is again greater and less variable than that of nonfiltered data (192 ± 29 pm). Compared to the negative control (i.e., the cellular responses to assay buffer only; 5 ± 9 pm, $n=48$), the Z' factor, a common assay robustness measure, was 0.74 and 0.40 for the filtered and nonfiltered data, respectively. These results suggest that it is possible to introduce an intrawell filtration method to increase assay robustness when needed.

However, the histamine DMR amplitude of the confluent monolayer (309 ± 16 pm) is still significantly higher than that of partially confluent cells after data filtration (239 ± 16 pm). One possibility is the difference in receptor biology (thus ligand pharmacology) for cells with different confluencies. To examine this, the cells in columns 7–12 were stimulated with histamine at $2\times$ dilution series of 16 doses down from $32 \mu\text{M}$. Figure 3 shows the dose-dependent histamine responses. Results show that histamine displayed cell confluency dependent potencies, and its EC_{50} was $1.67 \pm 0.32 \mu\text{M}$ and $3.90 \pm 0.43 \mu\text{M}$ ($n=3$) for fully and partially confluent cells, respectively. However, the

maximum responses were statistically the same. This explains the difference in DMR amplitude of histamine at $5 \mu\text{M}$ observed in Fig. 2. The histamine of $5 \mu\text{M}$ equals to its EC_{80} and EC_{65} values for fully and partially confluent cells, respectively. These results suggest that although the ligand potency may be somewhat sensitive to cell confluency, the data filtration can be applied to improve screening data quality when the agonist at slightly higher doses (e.g., EC_{100}) is used.

In conclusion, we have developed a RWG imager that enables the simultaneous imaging of all biosensors within a microtiter plate. The imager has moderate spatial resolution ($80 \mu\text{m}$), high data acquisition rate (~ 3 s), and good thermal noise (0.2 pm) under ambient conditions. The imager is well tolerant to artifacts in plate geometry and configurations if any. Given appropriate concentrations of ligands used, a simple data filtration protocol can be used to improve assay robustness when there is variability in cell confluency. Improvements in acquisition rate and spatial resolution will enable label-free imaging-based analysis at single cell level.¹⁶ Label-free assays at single cell resolution¹⁷ will open next dimensions for studying cell biology, particularly cancer biology and cell reprogramming where heterogeneity in cell populations and cell signaling is critical.

This work was supported partially by National Institutes of Health under Grant 5U54MH084691 (Y.F.).

- ¹Y. Fang, A. G. Frutos, and R. Verklereen, *Comb. Chem. High Throughput Screening* **11**, 357 (2008).
- ²T. Kenakin, *Nat. Rev. Drug Discovery* **8**, 617 (2009).
- ³Y. Fang, "Label-free receptor assays," *Drug Discovery Today: Technologies* (in press).
- ⁴Y. Fang, G. Li, and J. Peng, *FEBS Lett.* **579**, 6365 (2005).
- ⁵Y. Fang, A. M. Ferrie, N. H. Fontaine, and P. K. Yuen, *Anal. Chem.* **77**, 5720 (2005).
- ⁶Y. Fang, A. M. Ferrie, N. H. Fontaine, J. Mauro, and J. Balakrishnan, *Biophys. J.* **91**, 1925 (2006).
- ⁷Y. Fang, G. Li, and A. M. Ferrie, *J. Pharmacol. Toxicol. Methods* **55**, 314 (2007).
- ⁸Y. Fang and A. M. Ferrie, *FEBS Lett.* **582**, 558 (2008).
- ⁹A. Kebabian, E. Kostenis, K. Mohr, and M. Mohr-Andra, *Recept Signal Transduct* **29**, 140 (2009).
- ¹⁰C. M. Henstridge, N. A. B. Balenga, R. Schroder, J. K. Kargl, W. Platzer, L. Martini, S. Arthur, J. Penman, J. L. Whistler, E. Kostenis, M. Waldhoer, and A. J. Irving, *Br. J. Pharmacol.* **160**, 604 (2010).
- ¹¹M. F. Peters, F. Vaillancourt, M. Heroux, M. Valiquette, and C. W. Scott, *Assay Drug Dev. Technol.* **8**, 219 (2010).
- ¹²Y. Fang, *Sensors* **7**, 2316 (2007).
- ¹³Y. Fang, *Assay Drug Dev. Technol.* **4**, 583 (2006).
- ¹⁴E. Tran and Y. Fang, *J. Biomol. Screening* **13**, 975 (2008).
- ¹⁵J. J. Ramsden, S. Y. Li, J. E. Prenosil, and E. Heinzle, *Cytometry* **19**, 97 (1995).
- ¹⁶Y. Fang, A. M. Ferrie, and Q. Wu, U.S. Patent Application No. US20090093013A1.
- ¹⁷Y. Yanase, T. Hiragun, S. Kaneko, H. J. Gould, M. W. Greaves, and M. Hide, *Biosens. Bioelectron.* **26**, 674 (2010).